Application of Optical Flow and Scale Space Methods to Sea-Ice Motion in Antarctica

Salvador Gutiérrez and David G. Long

Brigham Young University, 459 Clyde Building, Provo, UT 84602, USA

ABSTRACT

Methods from computer vision and scale-space theory are applied to the study of sea-ice motion in Antarctica. The input data is a sequence of daily images of the continent, obtained from scatterometer data and processed with a resolution enhancing algorithm. The information contained in these images can be studied at different scales when the appropriate filters are applied. Large scales omit detail and smoothen local variations of intensity while smaller scales show much detail and local variation. When motion is studied through different scales, different patterns might be observed. We assume that all the information coded in these images is the radar backscatter, and that it is closely coupled with advection. The Optical Flow method is used to obtain a dense vector field representing sea-ice motion, the method's limitations are overcome by adding second order constraints to the main equation and through the use of large neighborhoods to normalize the direction of flow.

Validation of results has been done to the extent possible, taking into account that there is practically no ground-truth data available for Antarctica in the form of buoy-data. Sea-ice motion results are displayed along available ocean surface wind data, observing a clear consistency along the ocean-ice border. The results are compared to existing studies applying wavelets and it is shown that differences can be explained by the fact that each method is observing motion at a different scale.

Keywords: sea-ice motion, scatterometer, QuikSCAT, ocean winds, optical flow, scale-space

1. INTRODUCTION

Motion patterns of sea ice are analyzed in Antarctica, using a sequence of images of the complete continent including the sea-ice cover, produced from satellite scatterometer data combining ascending and descending paths with a resolution-enhancing algorithm.[1] The scatterometer SeaWinds on QuikSCAT was originally designed to estimate ocean wind velocities and directions, but has been also successfully used to study sea-ice motion.[2] Each of the 21 daily images has 1940×1940 floating point pixels representing values of radar backscatter at a resolution of 4.45 km/pixel (see Fig. 1).

The size of the available images and the amount of information contained in them has led to consideration of the principles of scale-space theory in order to break their complexity down. The scale-space of each of these images was generated by applying gaussian low-pass filters.[3,4] In trying to discern motion patterns from the scale-space of the image sequence it is apparent that motion is *scale-dependent*. Features discerned by humans, or computed by an algorithm, can be seen to follow particular motion patterns at each scale, and these patterns are not necessarily the same for different scales.

We desire a dense vector field as the end product of our estimations, which has led us to consideration of Optical Flow (OF) methods. OF methodologies have been extensively studied in the context of computer vision applications, and have also been applied to remote sensing problems, such as sea-ice motion estimation.[5] The limitations of these methods are well known and have been considerably reduced in this study through the use of second order contraints and regularization.

Further author information: (Send correspondence to SG)
DGL: E-mail: long@ee.byu.edu, Telephone: 1 801 422 4383
SG: E-mail: salvador@cs.byu.edu, Telephone: 1 801 422 2195

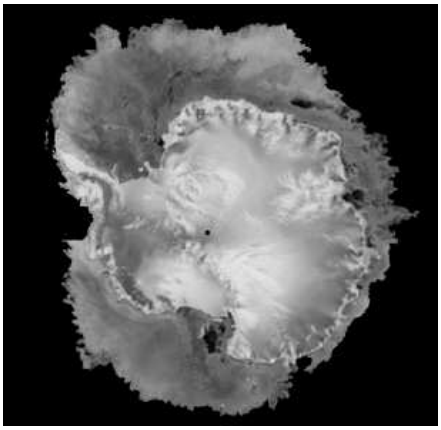

Figure 1. QuickSCAT one day backscatter imagery, 1940 × 1940 pixels, 4.45 km/pixel.

2. SCALE

The act of measuring an observable variable implies an aperture. The size of this aperture determines the measurement resolution, which is the average of the observed variable taken over the aperture. This implies that any feature of size smaller than the aperture cannot be observed. For any measurement there is an associated aperture in *space* and another in *time*. This precludes events with duration shorter than the time aperture from being observed.

Definition of the appropriate scales (spatial and temporal), is as important as the definition of a reference frame when designing an experiment, or even when defining the object of observation. In our case, the observed variable is σ°, and the intrinsic apertures are determined by the instrument's characteristics (antenna footstep size and form, rotation rate, satellite speed, etc.), and by all the processes that result in a production quality image (distortion removal, denoising, resolution enhancing, ocean- or ice-masking, cartographic projection, etc.).

Starting from such an image we must assume that it contains all available information and that processing cannot increase the amount of information that it originally had. However, we may *decompose* the complexity of such an image by generating its *scale-space*, which is a multi-scale representation of a signal achieved by convolution with gaussian low pass filters with different support sizes. This representation is tied to a scale parameter, which in this case is the standard deviation of the corresponding gaussian filter. Four points of the scale space of a subimage, with corresponding linear features superposed (derived by finding the maximum of the gradient in the direction of the gradient at different scales), can be seen in Fig. 2.

At a given value of the scale parameter, the effective aperture is determined by the size of the corresponding convolution kernel and features of lesser size have been eliminated (or rather *averaged out*). If convolution is made along the *time* dimension, the temporal aperture effectively preclude all events of shorter duration from being observed.

Motion patterns can be extracted from a sequence of images at a given consistent scale parameter value. In this way motion can be studied also in a scale-space. It is interesting to see that motion patterns at different scales do not need to be the same (see Fig. 3).

3. EXISTING METHODOLOGY

Among the standard methodology applied to sea-ice motion estimation in Antarctica are the correlation-based methods, Maximum Cross Correlation[6] and Nested Correlations,[7] which determine sea-ice motion to an implicit scale determined by the size of the correlation window. These methods, as all others, must provide a way to deal with problems such as weather induced intensity changes from one frame to another, distinction between ice motion and melting or ice growth, convergent and divergent motion.

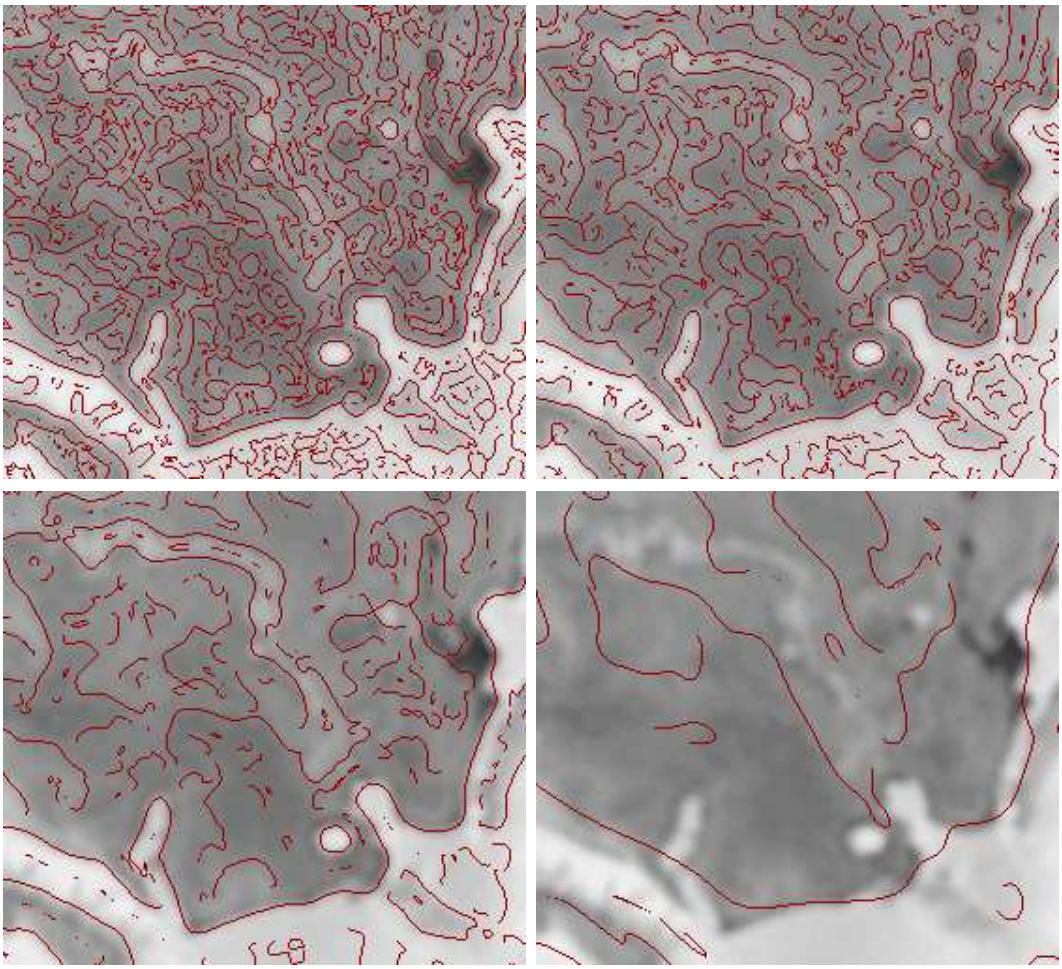

Figure 2. Linear features computed at different scales, from top to bottom and left to right, they are respectively, 12, 24, 48 and 168 pixels.

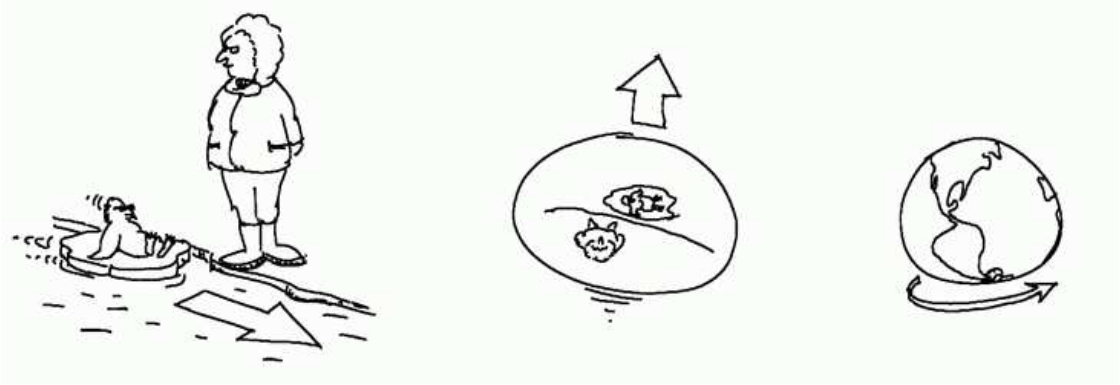

Figure 3. Motion relativity to scale. At a small scale in space and time, an observer might perceive some object traveling from right to left according to his reference frame (see drawing in left). Someone flying an aircraft would observe this at a larger scale in space and time (see center), and would perceive that observer, penguin and the ice and water they are on, are actually moving in another direction. This motion is longer lived than the previous one and the prevalent motion is that indicated by the arrow. A third observer from a spacecraft would perceive motion in an even larger time and space scale, and would see that everything is moving east, as the Earth rotates. This motion is even longer lived than the previous ones and would have a different direction. As a consequence, when observing motion, consideration to the spatio-temporal scale is crucial.

Another methodology that has been applied to the same problem is the wavelet approach,[8–10] where wavelets implement the Laplacian (or "Mexican Hat") filter to an image, producing features that are tracked by template matching. This method also determines motion to an implicit scale determined by the support of the Laplacian filter and the peculiarities of the template matching stage.

4. OPTICAL FLOW (OF)

OF methods stem from Horn's restrictive equation,[11] which represents the assumption that the intensity and shape of a moving neighborhood on the observed object remain invariant in a short interval. It can be written as the total derivative of an intensity function

$$\frac{\mathbf{D}I}{dt} = \frac{\partial I}{\partial x}\frac{dx}{dt} + \frac{\partial I}{\partial y}\frac{dy}{dt} + \frac{dI}{dt} = \nabla_s I \cdot \mathbf{u} + I_t = 0 \tag{1}$$

where $\mathbf{u} \equiv \left(\frac{dx}{dt}, \frac{dy}{dt}\right)^T$, $I_t \equiv \frac{d}{dt}I$ and s is the scale parameter. The derivatives $\frac{\partial I}{\partial x}$, $\frac{\partial I}{\partial y}$ and $\frac{d}{dt}I$ are computed by convolution with corresponding gaussian derivative kernels in space and time, leaving $\frac{dx}{dt}$ and $\frac{dy}{dt}$ as unknowns.

Since there is only one equation with two unknowns this relation is underconstrained, although a least-squares solution may be found by taking points in a neighborhood. However, as is evident from equation (1), only the OF component in the direction of the gradient can be determined. This is known as the *aperture problem.*

Further constraints should be added to alleviate this problem, we follow the approach taken in Ref.,[12] imposing a second order constraint by observing that if $\frac{\mathbf{D}}{dt}I$ vanishes, then higher order total derivatives must also vanish. In particular, $\frac{d^2}{dt^2}I = 0$ which implies that $\frac{\partial}{\partial t}\nabla I \cdot \mathbf{u} + \nabla I \cdot \frac{\partial}{\partial t}\mathbf{u} + \frac{\partial^2}{\partial t^2}I = 0$. When $\frac{\partial}{\partial t}\mathbf{u} \to 0$ and $\frac{\partial^2}{\partial t^2}I \to 0$, these relations for each pixel in a certain neighborhood, give a system of equations whose least squares solution yields the OF.

The field is regularized through a normalization approach, computing the least squares solution with large neighborhoods (we used a circular neighborhood with a diameter of 30 pixels). This regularizes the OF directions field but results in smaller magnitudes because more points contributing in different directions are included, reducing the magnitude of the estimated resultant $\mathbf{u}$. In other words, uncertainty in the magnitude of the displacement is traded for a more robust estimator of the motion direction, reducing the aperture problem. We

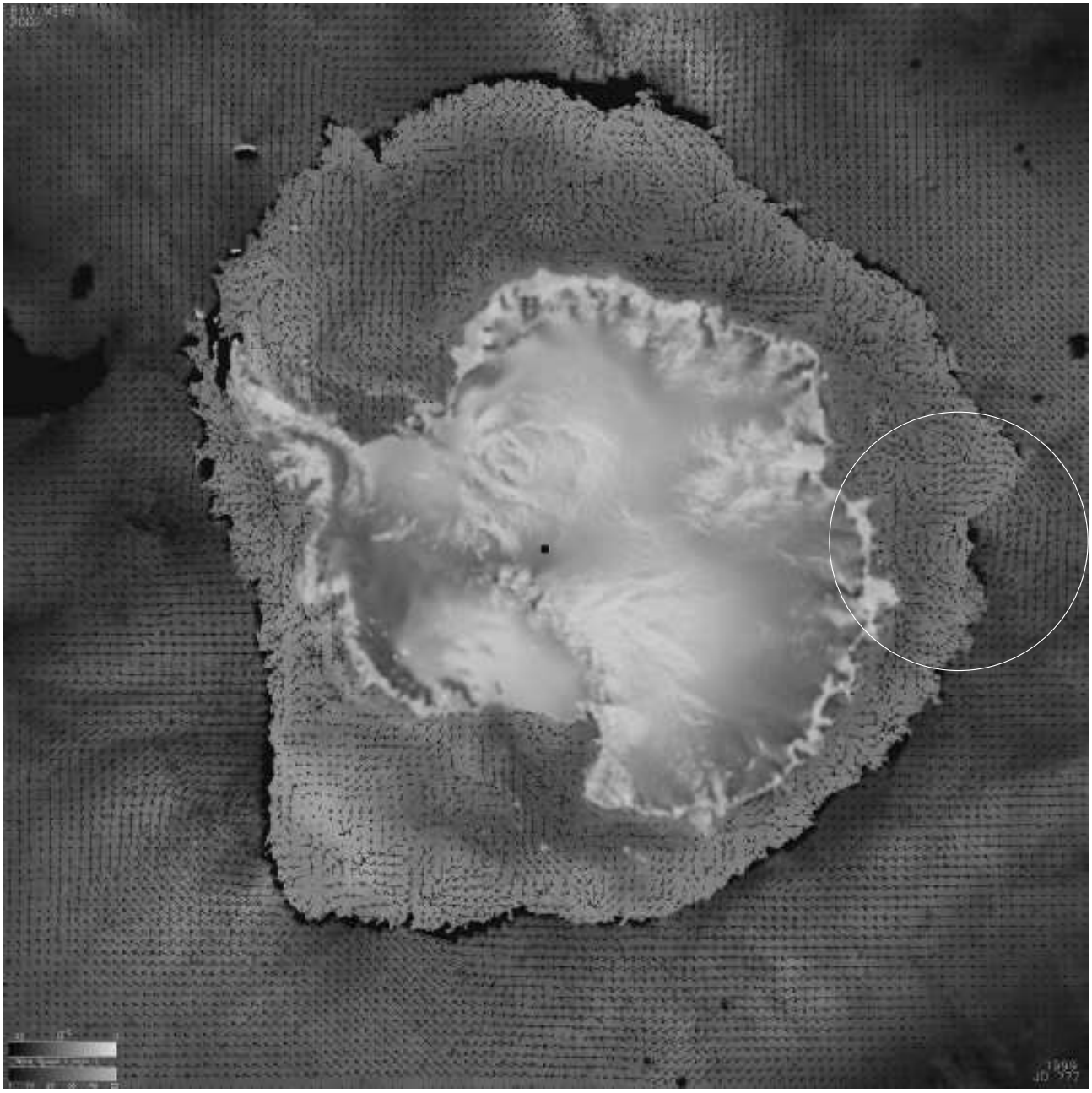

Figure 4. OF sea-ice motion data (on sea ice mantle) combined with ocean near-to-surface winds. Arrows over sea-ice are OF estimates; arrows over the ocean are JPL's QuikSCAT L3B sea winds data. The image corresponds to Julian date 277. The white circle contains a storm pattern which is halfway over sea ice and over the ocean.

note that OF methods are subject to the same problems mentioned in Section 3, but result in a dense vector field which can be easily interpolated to sub-pixel precision.

5. RESULTS

An estimate of the motion vector field over Antarctica can be seen in Fig. 4, where it is combined with JPL's QuikSCAT L3B winds data over an image of the continent, including surrounding sea ice and ocean. Both data

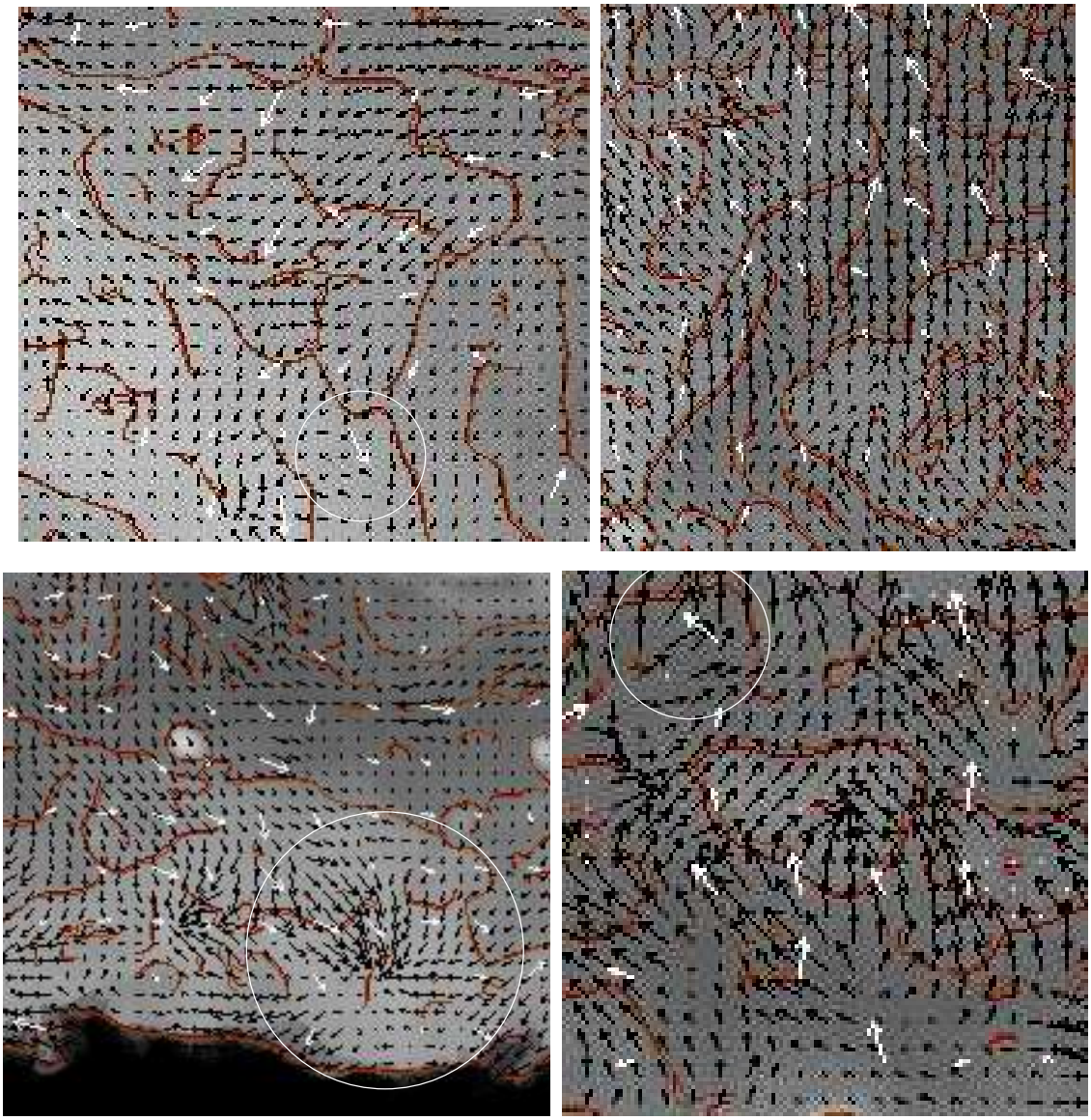

Figure 5. OF estimation data (black arrows) and data from the wavelet method (white arrows), overlaying a v-pol σ° image. Darker curvilinear features correspond to Julian day 277, 1999, whereas the lighter ones correspond to Julian day 278, 1999. The white arrows appear to represent motion at a larger scale, whereas the black arrows follow closer at a smaller scale. See discussion in section 5.

sets are consistent along the border of the ocean-sea ice interface, especially in regions such as eastern Antarctica, where it is possible to discern a storm's spiral pattern, which is half over sea ice and half over the ocean. While this fact does not validate OF sea-ice motion data it demonstrates that both data sets are consistent, since strong winds tend to influence sea ice motion.

Estimates of sea-ice motion from the wavelet method and from the OF data are compared using three distinct measures of difference: The average euclidean difference (AED), the average angular difference (AAD), and the root mean square difference (RMS). These measures are defined as follows, if $\mathbf{z} = \mathbf{x} - \mathbf{y}$ is the difference vector between observations, then

$$AED(\mathbf{z}) = \frac{1}{M}\sum_{i=1}^{M} \|\mathbf{z}_i\| \tag{2}$$

$$AAD(\mathbf{x},\mathbf{y}) = \frac{1}{M}\sum_{i=1}^{M} \arccos\left(\frac{\mathbf{x}_i' \cdot \mathbf{y}_i}{\|\mathbf{x}_i\|\ \|\mathbf{y}_i\|}\right) \tag{3}$$

$$RMS(\mathbf{z}) = \left(\frac{1}{M}\sum_{i=1}^{M} \|\mathbf{z}_i\|^2\right)^{\frac{1}{2}}. \tag{4}$$

The AED is an intuitive difference measure, being the average difference in magnitude. The AAD gives an idea of the differences in orientation and the RMS is dependent on the magnitudes of the vectors, but was included because it is a commonly used measure.

OF sea-ice motion data are compared to estimates computed with the wavelet method and are found to differ significantly (see Table 1), but the differences can be explained by arguing that both data sets are looking at the same motion with different intrinsic observational scales. Table 1 shows that the differences get smaller as the scale increases, suggesting that the wavelet data corresponds to a larger scale. Figure 5 shows four different areas of Antarctica's sea ice mantle with both ice motion data sets displayed simultaneously. An overall agreement can be appreciated in most regions, places where differences are significant are highlighted with white circles. The top-left insert shows generally good agreement of both data sets, except where indicated by the white circle. This difference could be caused by assuming the white arrows to depict a larger scale flow. In the top-right insert both flows are consistent with the displacements shown by the curvilinear features. It can be seen that the black arrows depict a pattern with a smaller scale. The bottom-right insert shows a similar situation, and even when both data sets disagree strongly as inside the white circle, both are consistent with the observed displacements of the curvilinear features if a larger scale is assumed for the white arrow flow. In the left-bottom insert the black arrows form a convergent pattern, whereas the white arrows do not. This may happen if the wavelet method is using a scale larger than the converging pattern, or if its template matching stage is cannot handle convergent flows.

A complete validation is difficult because there is insufficient ground-truth in the form of buoy data in Antarctica. When this data become available it will be necessary order to match the effective scales of the methods being validated.

6. SUMMARY

A new method to estimate sea-ice motion is proposed, which offers a dense vector field, in contrast to existing methods which result in sparse fields. The new method provides the possibility of studying motion patterns in different observational scales in a systematic and controlled way. We note that a given motion pattern looks different when observed at different scales, and that it is necessary to match the scales of different observations before a fair comparison can be made. OF methods are known to have some limitations like the aperture problem, but these limitations can be overcome with adequate constraining of the method and with regularization of the direction field. An advantage of OF methods is that they can be applied in different scales by control of a single scale parameter. Complete validation of OF (and of any other) methods must wait until there is adequate buoy data from Antarctica. Further, results must be compared with compatible scales.

Table 1. Difference between wavelet and OF estimates of motion velocity, JD 277, 1999.

Neighborhood rad.	15 pix	30 pix	60 pix
AED (pixels/day)	3.7	3.6	3.7
AAD (degrees)	64.3°	59.8°	58.7°
RMS (pixels/day)	4.4	4.4	4.5
Number of points	1,120	1,108	1,108

ACKNOWLEDGMENTS

SeaWinds data was obtained from the Physical Oceanography Distributed Data Archive (PO.DAAC) at the CalTech Jet Propulsion Laboratory.

REFERENCES

1. D. S. Early and D. G. Long, "Image reconstruction and enhanced resolution imaging from irregular samples," *IEEE Transactions on Geoscience and Remote Sensing* **39**, pp. 291–302, Feb 2001.
2. D. G. Long and M. R. Drinkwater, "Cryosphere applications of NSCAT data," *IEEE Transactions on Geoscience and Remote Sensing* **37**, pp. 1671–1684, May 1999.
3. B. M. ter Haar Romeny, ed., *Geometry-Driven Diffusion in Computer Vision*, Kluwer Academic Publishers, Dordrecht, The Netherlands, 1994.
4. M. Nielsen, L. Florack, and R. Deriche, "Regularization and scale space," Tech. Rep. 2352, INRIA, Sep 1994.
5. Q. Yang, B. Parvin, and A. Mariano, "Detection of Vortices and Saddle Points in SST Data," *Geophysical Research Letters* , 2001.
6. W. Emery, C. Fowler, and J. Maslanik, "Satellite-derived maps of Arctic and Antarctic sea ice motion: 1988 to 1994," *Geophysical Research Letters* **24**(8), pp. 897–900, 1997.
7. M. Fily and D. Rothrock, "Sea ice tracking by nested correlations," *IEEE Transactions on Geoscience and Remote Sensing* , 87.
8. A. Liu, Y. Zhao, and S. Wu, "Arctic sea ice drift from wavelet analysis of NSCAT and special sensor microwave imager data," *Journal of Geophysical Research* **104**, pp. 11529–11538, 1999.
9. A. Liu and D. Cavalieri, "On sea ice drift from the wavelet analysis of the defense meteorological satellite program (DMSP) special sensor microwave imager (SSM/I) data," *International Journal of Remote Sensing* **19**(7), pp. 1415–1423, 1998.
10. Y. Zhao, A. K. Liu, and D. G. Long, "Validation of Sea Ice motion from QuikSCAT with those from SSM/I and buoy," *IEEE Transactions on Geoscience and Remote Sensing* **40**, pp. 1241–1246, Jun 2002.
11. B. K. P. Horn, *Robot Vision*, The MIT Press, 1986.
12. H. F. (Shekarforoush), "A closed-form solution for optical flow by imposing temporal constraints," in *IEEE International Conference on Image Processing*, **3**, pp. 656–659, 2001.